Kinetics of Isotropic–Smectic Phase Transition in Liquid-Crystalline Polyethers

Håkan Jonsson, Elisabet Wallgren, Anders Hult, and Ulf W. Gedde*

Department of Polymer Technology, The Royal Institute of Technology, S-100 44 Stockholm, Sweden. *Received May 30, 1989; Revised Manuscript Received August 11, 1989*

ABSTRACT: The isotropic–smectic mesophase (ism) transition in two thermotropic main-chain polyethers based on bis(4-hydroxyphenoxy)-*p*-xylene and two different methylene spacers with 9 and 11 carbons, respectively, have been studied under isothermal conditions by polarized-light microscopy and differential scanning calorimetry. The ism transition, which displays all the characteristics of a nucleation controlled process, follows the general Avrami equation with an exponent typically between 2.5 and 3.0. The growth rate (dL/dt) of the mesomorphic mosaic domains, which is greater along than perpendicular to the chain axis, is, at isothermal conditions, constant with time and follows $dL/dt = C_1 e^{-K_g/T(T_i-T)}$ where C_1 and K_g are constants and T_i is the equilibrium clearing temperature. DSC data revealing the overall rate are consistent with this view. A second process which occurred at rates almost comparable with the ism transition at high temperatures displayed an Arrhenius type temperature dependence with an activation energy of about 400–850 kJ mol^{-1}. This is indicative of a rearrangement, e.g., a perfection of the smectic mesophase occurring without nucleation. This process followed the Avrami equation with an exponent of about 2.0–2.2.

Introduction

There have been only very few reports, e.g., ref 1–4, dealing with the kinetics of isotropic–mesomorphic state (im) transitions in polymers. Bhattacharya et al.[1] showed by DSC that for a main-chain polyester based on 1,10-bis[[*p*-(chloroformyl)benzoyl]oxy]decane and 2-propyl hydroquinone the transition from the isotropic to the nematic state followed the Avrami equation with an Avrami exponent equal to 1.0, which is indicative of one-dimensional growth. Liu et al.[2] reported the same value for a similar polymer, an aromatic polyester based on 1,10-bis[[(chloroformyl)benzoyl]oxy]decane and 2-formyl-1,4-dihydroxybenzene. Hans and Zugenmaier[3] studied by polarized-light microscopy a side-chain LC polymer with an atactic poly(methacrylate) backbone and side chains with biphenyl groups as mesogens, connected to the main chain via an $-O(C_6H_{12})O-$ group. A transition from an isotropic melt to a smectic mesophase was established.[3] It was also shown that this transition followed the general Avrami equation with an exponent equal to 1.8–1.9,[3] indicating a two-dimensional mesophase growth following an athermal nucleation event. For another side-chain polymer, poly(*p*-biphenylyl acrylate), Pracella et al.[4] reported an Avrami exponent equal to about 3 for the isotropic to smectic A transition. Low molar mass liquid-crystalline compounds have been studied more, and for cholesteryl derivates it has been shown that the transition from isotropic to cholesteric phase is nucleation controlled and follows the general Avrami equation with an exponent close to 2.[5–7]

A difficult problem when studying main-chain polyesters is that they often degrade before reaching the high temperatures necessary for kinetic studies. In this paper we therefore present kinetic data on the im transition for two main-chain polyethers. These polymers, which are based on bis(4-hydroxyphenoxy)-*p*-xylene and two different methylene spacers with 9 and 11 carbons, respectively, are stable at temperatures above their clearing temperature.[8] It was shown in the first paper on these polymers[8] that they form a smectic phase directly from the isotropic melt and that a smectic–solid crystal transition occurs at a temperature about 25 K lower.

Experimental Section

Sample Preparation and Characterization. Two liquid-crystalline polyethers based on bis(4-hydroxyphenoxy)-*p*-xylene and two different methylene spacers with 9 and 11 carbons, respectively (HPX-C9 and HPX-C11), were prepared by a phase-transfer-catalyzed Williamson ether synthesis. Details from the preparation of these polymers are presented in ref 8. The structure of the polymers is as follows:

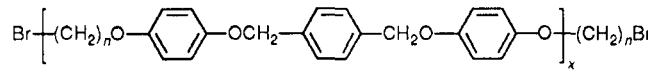

$n = 9, 11$

The number average molecular weights determined by end-group analysis were M_n = 9700 (HPX-C9), 10 300 (HPX-C11 no. 1), and 6300 (HPX-C11 no. 2).

The molecular weight of HPX-C11 no. 2 was also determined by gel permeation chromatography (Waters 200 GPC) at 408 K, using trichlorobenzene as eluent: M_n = 6300 and M_w = 15 600. The GPC data were analyzed using the universal calibration procedure with estimated values for the Mark–Houwink parameters (a = 1.2) for this semirigid polymer.

Studies of Kinetics. The kinetic studies of the isotropic–smectic phase transition have been carried out by polarized-light microscopy (Leitz Ortholux POL BK II equipped with crossed polarizers and a temperature-calibrated Mettler hot-stage FP 82) and DSC (Perkin-Elmer DSC-2 and DSC-7, temperature and energy calibrated according to standard procedures).

Polarized-light microscopy was performed in the hot stage by cooling (20 K min^{-1}) the 10-μm-thick samples from 488 K (HPX-C9) and 478 K (HPX-C11) to the experimental isothermal temperature (T) followed by photographic recording at different times (t) after the establishment of isothermal conditions. The samples were kept at the maximum temperature (488 and 478 K, respectively) for 1 min. A linear relationship was in all cases established between the dimensions of the mesomorphic domains and t. By measurement of at least 10 growing mesomorphic domains/sample at each temperature, a mean value for the linear growth rate (G) was determined. The directional dependence of G with respect to the director (direction for greatest refractive index) was also studied by inserting a λ

* To whom correspondence should be addressed.

0024-9297/90/2223-1041$02.50/0

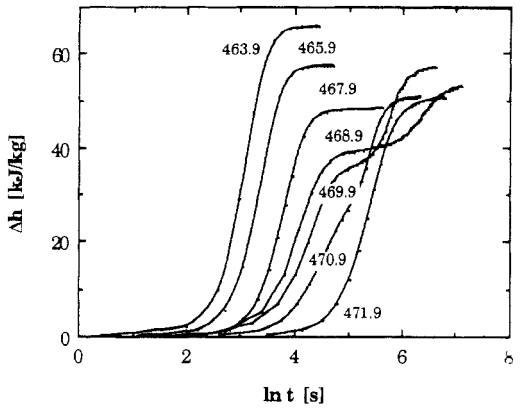

Figure 1. Exothermal heat (Δh) developed in HPX-C9 as a function of time (t) at different temperatures (in K).

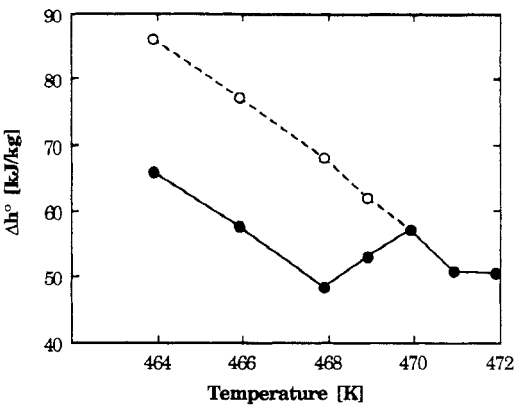

Figure 2. Total heat ($\Delta h°$) recorded under isothermal conditions in the DSC for HPX-C9 plotted versus temperature: measured values (●); corrected values (○).

plate in the beam. After the isothermal treatments, the samples were heated at a rate of 1 K min^{-1} in the hot stage to reveal the clearing temperature (T_i).

Samples weighing about 5 mg were cooled in the DSC apparatus at a rate of 80 K min^{-1} from 485 K to the experimental isothermal temperature (T), and the exotherm associated with the first-order transition was recorded during the isothermal conditions. The samples were kept at the maximum temperature (485 K) for 1 min. These data were analyzed according to the general Avrami equation

$$1 - \Delta h/\Delta h° = e^{(-Kt^n)} \quad (1)$$

where Δh is the integral heat developed in the process during time t, $\Delta h°$ is the total heat involved in the process, K and n are the parameters to be determined, and t is the time, which is set equal to zero at the very start of the exothermal process. After the isothermal treatment a few of the samples were cooled to 293 K at a rate of 5 K min^{-1} while the exothermal process associated with crystallization was recorded.

Results and Discussion

Figure 1 presents a summary of the calorimetric data for HPX-C9. The behavior of the HPX-C11 polymer were similar. Two processes are in fact revealed by these data: (a) At high temperatures ($T \geq 471.9$ K) the two processes have approximately the same induction time and rate and are therefore not resolved. (b) At intermediate temperatures ($468.9 \leq T \leq 470.9$ K) the two processes are clearly resolved and the heat evolved in the slower process is 30–50% of that evolved in the more rapid process. There is a tendency for an increase in $\Delta h°$ for the slow process with increasing temperature; for HPX-C9, $\Delta h°$ was equal to 13 kJ kg^{-1} at 468.9 K and 20 kJ kg^{-1} at 470.9 K. The same trend was observed for HPX-C11. (c) At low temperatures ($T \leq 467.9$ K), the slower process was much retarded and not observed within the experimental window.

The solid line in Figure 2 shows the total heat ($\Delta h°$) involved in the two processes. It is clear that $\Delta h°$ decreases with increasing temperature over the whole temperature range, although there is a narrow temperature region, for HPX-C9 between 467.9 and 469.9 K, in which $\Delta h°$ increases with increasing temperature. The reason for this increase in $\Delta h°$ is related to the definition of this quantity and to the limited experimental potential for detecting very slow processes. At temperatures less than 467.9 K, the slower process in not recorded and the $\Delta h°$ value measured is only that associated with the rapid process, whereas at higher temperatures the $\Delta h°$ values partially or fully include the contribution from the second slower process. Hence, if the total contribution from the second slower process were included in $\Delta h°$ at the lower temperatures, the broken curve in Figure 2 would be obtained, on the assumption that $\Delta h°$ for the slower process is 20 kJ kg^{-1} throughout the experimental temperature range. The same monotonic decrease in the total $\Delta h°$ with increasing temperature was obtained for HPX-C11.

There are at least two plausible reasons for this decrease in $\Delta h°$, both related to the multicomponent character of the polymer. In the first place, the chain-length polydispersity of the samples is evident from the GPC data (see the Experimental Section). Another possible source of heterogeneity, not experimentally verified, is a variation in the sequence distribution of mesogenic and spacer groups in different molecules. This variation arises when two spacer groups couple via an ether linkage, due to displacement of the electrophilic chain end by OH^{-}[9]. The molecular weight distribution itself is however sufficient to explain the decrease in $\Delta h°$ with temperature. Percec et al.[10] have shown that the clearing temperature of a similar LC polyether increases with molecular weight. At high temperatures only a small fraction, the longer chains, of the sample is transformed into the mesophase, and with decreasing temperature a progressively larger fraction has the thermodynamic potential for transformation to the mesomorphic state.

Figure 3 presents a series of thermograms recorded under different cooling rates (1–100 K min^{-1}) from the isotropic melt. Three exothermal peaks were resolved at the lowest cooling rate. The high-temperature peak is associated with the formation of the mesophase. The origin of the low-temperature peaks has not yet been established, but at least one of them is associated with crystallization. X-ray diffraction data presented in a previous paper[8] show that these samples display crystalline Bragg reflections at room temperature. The presence of the two low-temperature peaks in the HPX-C11 sample after isothermal treatment at 463 K is an important observation (Figure 3). They clearly demonstrate that the low-temperature exothermal processes are not equivalent to the slow process recorded under isothermal conditions.

The establishment of an equilibrium transition temperature is essential for the kinetic studies of the phase transition. The equilibrium clearing temperature ($T°_i$) may be determined on the basis of the graph shown in Figure 4 by analogy with the commonly used Hoffman–Weeks plot.[11] The extrapolation of the $T - T_i$ data to $T = T_i = T°_i$ was simplified by the fact that T_i is almost independent of the temperature at which the mesophase was formed (Figure 4). The values for $T°_i$ obtained by this extrapolation were the following: HPX-C9, 482 K; HPX-C11 no. 1 and HPX-C11 no. 2, 474 K.

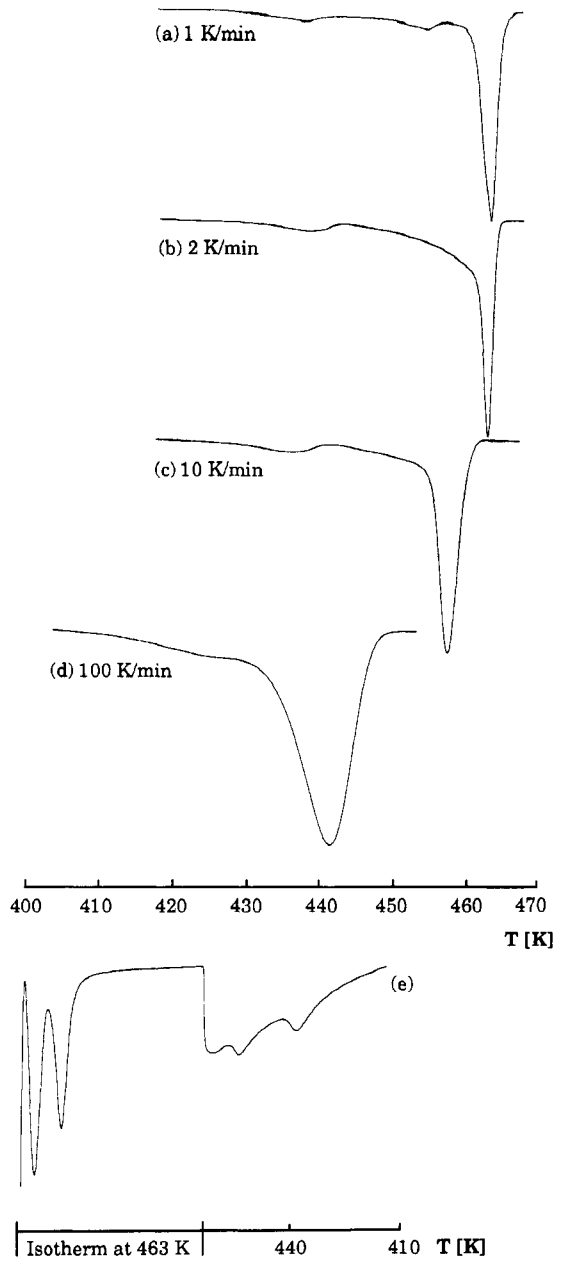

Figure 3. Thermograms obtained by cooling the HPX-C11 no. 2 samples from above the clearing temperature at different cooling rates. Curve (e) is the thermogram for a sample that was kept at 463 K for 10 min and then cooled at 5 K min^{-1} to 300 K.

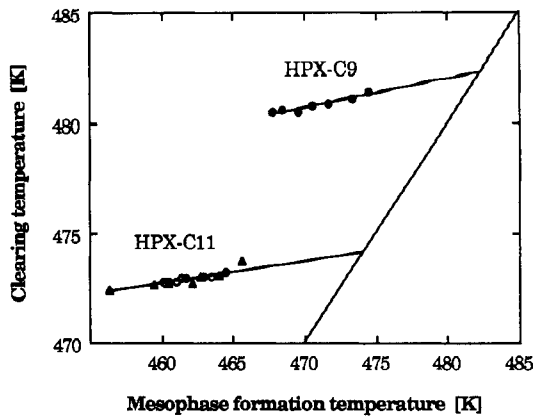

Figure 4. Clearing temperature (T_i) revealed by polarized-light microscopy as a function of the temperature (T) at which the mesophase has been formed. The extrapolations of the data revealing the equilibrium clearing temperatures ($T°_i$) are shown in the figure: HPX-C9 (●); HPX-C11 no. 1 (○); HPX-C11 no. 2 (▲).

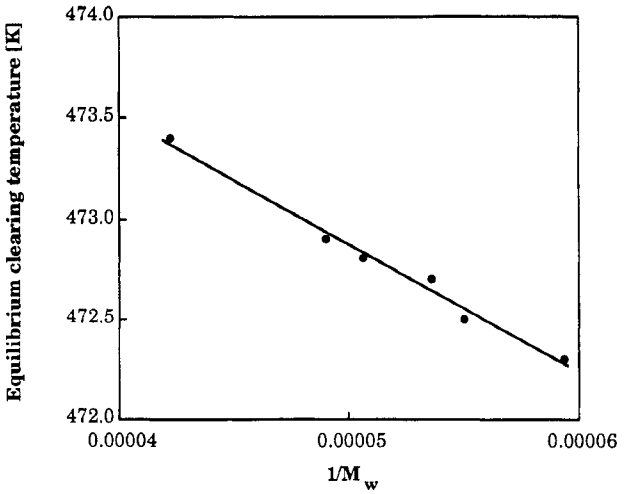

Figure 5. Equilibrium clearing temperature, $T°_i$, plotted versus the reciprocal of the weight average molecular weight ($1/M_w$) for HPX-C11 no. 2.

Table I
Phase Transition Kinetics

polymer	K_g (DSC)[a]	$\langle K_g \rangle$ (micr)[b]	K_{gc} (micr)[c]	K_{gp} (micr)[d]
HPX-C9	21 600	23 600		
HPX-C11	26 000	28 400	23 000	33 800

[a]From DSC according to eq 8. [b]Mean value, from polarized-light microscopy according to eq 7. [c]Growth in chain axis direction, from polarized-light microscopy according to eq 7. [d]Growth perpendicular to chain axis direction, from polarized-light microscopy according to eq 7.

There is one important flaw in the treatment of $T°_i$. The temperature dependence of $\Delta h°$ demonstrated in Figure 2 shows that only a fraction of the sample participates in the phase transition and that the molecular weight of this fraction possibly varies with temperature. Thus, the increase of T_i with increasing T may be associated with a decrease in concentration of chain-end defects, primarily because only a smaller fraction of the sample, i.e. higher molecular weight material, is transferred to the mesomorphic state with increasing temperature T. The following assumptions have been made in the analysis: (1) The fraction of sample transferred to the smectic mesophase is equal to the ratio $\Delta h(T)/\Delta h°$, where $\Delta h(T)$ is the total heat developed at temperature T and $\Delta h°$ is the heat associated with complete conversion, estimated by extrapolation of $\Delta h = f(T)$ data. (2) Only molecules with a molecular weight greater than a certain temperature-dependent critical value ($M_{crit}(T)$) can be transformed to the mesomorphic state. (3) The mesophase is composed of a mixture of molecules with $M > M_{crit}$, and its clearing temperature is controlled by the weight average molecular weight of this fraction.

This relationship between $T°_i$ and molecular weight (M) may be derived as follows:

The first question that has to be addressed is how the chains are arranged in the mesophase. At least two different structures exist: (1) that in which the chain ends are randomly distributed in the mesophase and (2) that in which the chain ends are located in layers, which means that the mesophase is broken down into thin lamellar submesophase domains. The broad molecular weight distribution, the rigid-rod nature of the chains, and the repulsive forces between the electronegative bromine end groups

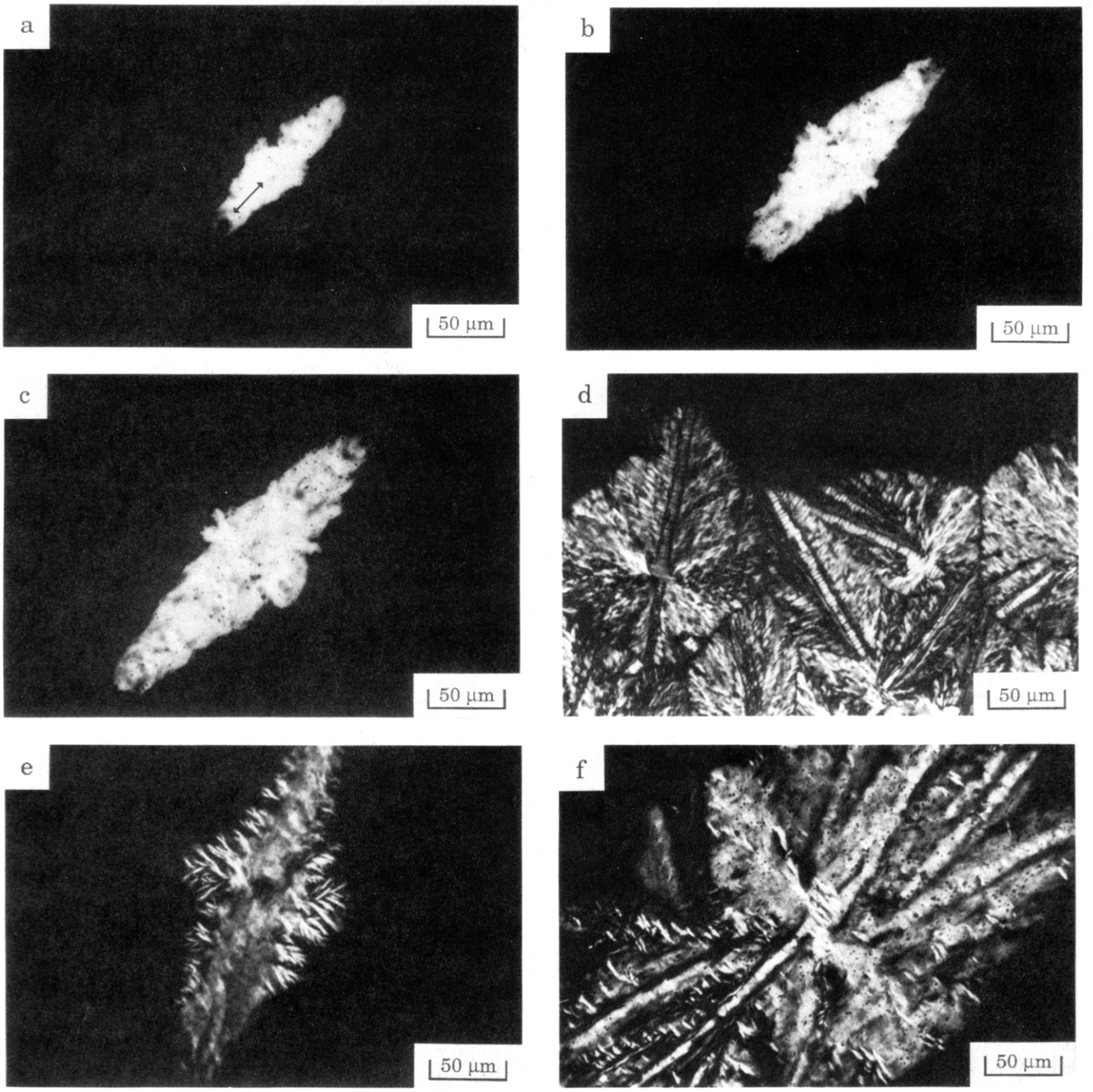

Figure 6. (a–c) Polarized photomicrographs of HPX-C11 no. 2 showing the growth of mesomorphic domains under isothermal conditions (464 K). The director (maximum refractive index), which is also the chain axis director, is shown in photomicrograph (a). (d–f) Morphologies of HPX-C11 no. 2 treated at the following temperatures: 459 K (d); 461 K (e); 462 K (f).

are factors in favor of the first model, although the clearing temperatures of both these structures possess a similar molecular weight dependence as is shown below.

The free energy change (Δg) associated with the formation of the smectic mesophase for a polymer of molecular weight M is given by the expression

$$\Delta g(M) = \Delta g(\infty) + 2\sigma/L\rho \tag{2}$$

where $\Delta g(\infty)$ is the free energy change for an infinitely large mesophase with no chain end defects, σ is the surface free energy associated with the vacancy in the mesophase caused by the chain end, L is the end-to-end distance of the molecule in the mesophase, and ρ is the density. It is here assumed that the chain ends are defects which cause vacancies and increase the free energy of the mesophase. In eq 2 this excess free energy is treated as a surface free energy σ associated with the cross-section of the molecular tube, regardless of whether model 1 or 2 applies.

The temperature dependence of Δg arises solely from $\Delta g(\infty)$:

$$\Delta g(\infty) = \Delta h^\circ[T^\circ_i(\infty) - T]/T^\circ_i(\infty) \tag{3}$$

Equation 3 assumes that the enthalpy change Δh° is constant with temperature; $T^\circ_i(\infty)$ is the equilibrium clearing temperature of a mesophase containing no chain end defects.

The end-to-end distance of the rigid-rod polymer in the mesophase is proportional to the molecular weight, so that

$$L = KM = L_{rep}(M/M_{rep}) \tag{4}$$

where L_{rep} is the length of the repeating unit in its con-

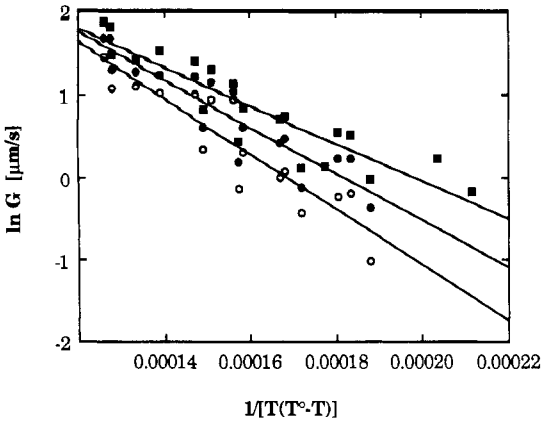

Figure 7. Logarithm of the linear growth rate G, based on polarized-light microscopy measurements, plotted versus $1/[T(T^\circ_i - T)]$ for HPX-C11 no. 2 (all samples): mean value (●); main direction (■); lateral (○).

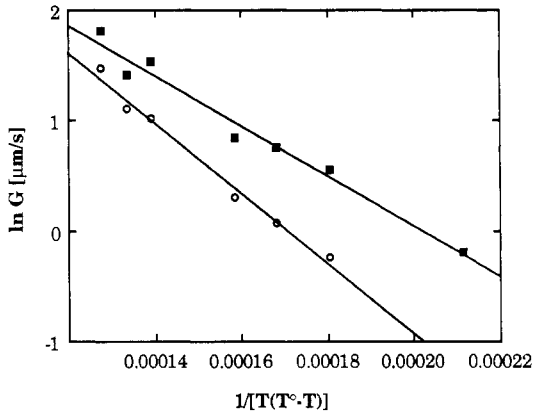

Figure 8. Logarithm of the linear growth rate G, based on polarized-light microscopy measurements, plotted versus $1/[T(T^\circ_i - T)]$ for HPX-C11 no. 2 (single sample): main direction (■); lateral (○).

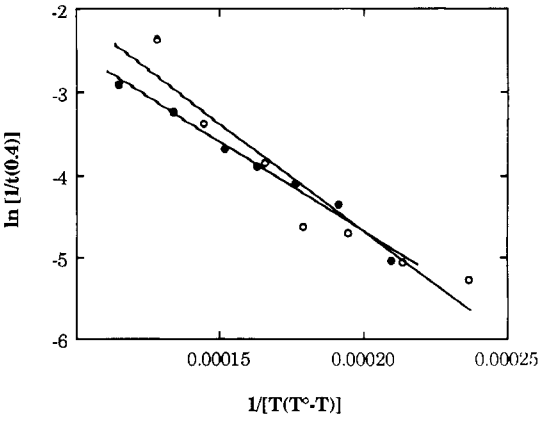

Figure 9. Logarithm of the reciprocal time for 40% conversion of the "rapid" process ln $(1/t_{0.4})$ plotted versus $1/[T(T^\circ_i - T)]$ for HPX-C9 (●) and HPX-C11 no. 1 (○).

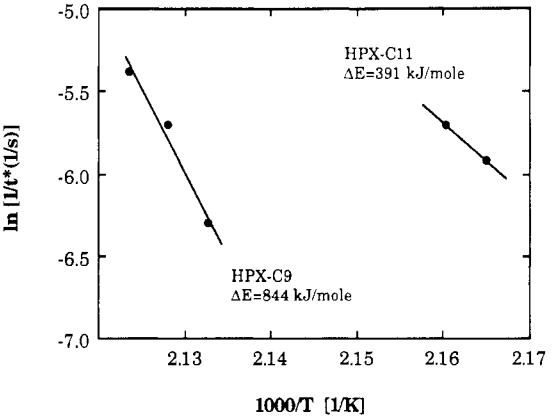

Figure 10. Arrhenius plot [ln $(1/t^*) = f(1/T)$, where t^* is the time at which the rate of the slower process is at a maximum] of the slow process for both HPX-C9 and HPX-C11 no. 1.

formation in the mesophase and M_{rep} is the molecular weight of the repeating unit.

Combination of eqs 2–4 yields the equation

$$\Delta g(M) = \Delta h^\circ[T^\circ_i(\infty) - T]/T^\circ_i(\infty) + 2\sigma M_{rep}/(L_{rep}M\rho) \quad (5)$$

and if eq 5 is set equal to zero, the equilibrium clearing temperature is obtained as

$$T^\circ_i(M) = T^\circ_i(\infty)[1 + 2\sigma M_{rep}/(L_{rep}M\rho\Delta h^\circ)] \quad (6)$$

Note that Δh° is negative and that eq 6 is analogous to the well-known Thomson–Gibbs equation.

When data for $T_i = f(T)$ and $\Delta h^\circ = f(T)$ and GPC data for the molecular weight distribution are combined, the data shown in Figure 5 are obtained.

The linear relationship between T°_i and $1/M_w$ predicted by eq 6 is here experimentally verified. Extrapolation of the data to $1/M_w = 0$ yields $T^\circ_i(\infty) = 476.1$ K. When appropriate values are inserted for the parameters in eq 5 ($M_{rep} = 474.64$ kg kmol^{-1}, $L_{rep} = 31.2 \times 10^{-10}$ m, $\rho = 1200$ kg m^{-3}, $\Delta h^\circ = 57$ kJ kg^{-1}), a surface free energy (σ) associated with the chain ends and equal to 53 mJ m^{-2} is obtained.

The equilibrium clearing temperature has been determined in two different ways. The first (according to Hoffman–Weeks) assumes that the equilibrium is attained when $T_i = T$ and disregards fractionation effects. The second assumes that the sample attains equilibrium at each temperature and that the increase in T_i with increasing T is due to fractionation. The difference between the different estimates of the equilibrium temperature is, however, relatively small, and the value later used for HPX-C11 (474 K) should be correct within 2 K.

The photomicrographs presented in Figure 6a–c show that the growth of the mesophase domains is dependent on direction and is more rapid along the direction of maximum refractive index. On all samples cooled to room temperature, linear cracks oriented parallel to the direction of maximum refractive index were observed. It is postulated that the direction of maximum refractive index is parallel to the domain director for the chain axis. The chain orientation within the mosaic domains is close to uniform as revealed by polarized-light microscopy. "Kink bands" involving a low-angle reorientation of the molecular director were occasionally observed in the mosaic domains. Thus, the growth rate is greatest in the chain axis direction and significantly lower in the perpendicular direction. The growth rate anisotropy is more significant at higher temperatures. This has relevance for the morphologies obtained at different temperatures. At high temperatures the mosaic domains become very long along the chain axis, whereas at low temperatures they become more quadratic. There is a range of different morphologies as shown in Figure 6a–f: At the lowest temperatures (HPX-C11 no. 2; 454–460 K) (Figure 6d), fibrillar structures with preferential chain orientation along the long axis are observed. The chain orientation of the material surrounding the fibrils is essentially perpendicular to the fibrillar long axis. At the highest temperatures (HPX-C11 no. 2; 461–464 K) (Figure 6a–c), mosaic domains of uniform chain orientation are the dominant morphol-

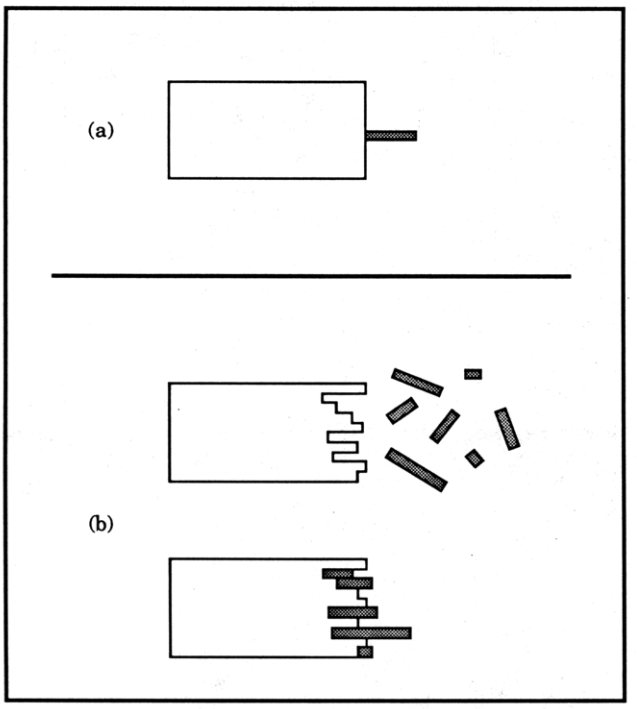

Figure 11. Schematic figure showing two models for the growth of the mesomorhic mosaic domains in the chain axis direction: (a) secondary nucleation from a smooth phase boundary; (b) the attachment of the rigid-rod chains on a rough phase boundary.

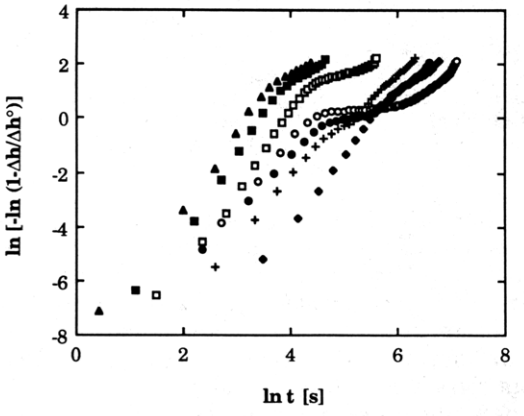

Figure 12. Avrami plots (according to eq 1) for HPX-C9 obtained at different temperatures: 463.9 K (▲); 465.9 K (■); 467.9 K (□); 468.9 K (○); 469.9 (●); 470.9 K (+); 471.9 K (◆).

ogy. In some cases, the mosaic domains exhibit a dendritic substructure (Figure 6e). At intermediate temperatures (HPX-C11 no. 2; 460–462 K), a combination of fibrillar and the mosaic structures are observed (Figure 6f). The main growth direction is nevertheless along the chain axis of the molecules.

Figure 7–10 present the rates of the two processes as a function of temperature. The rapid process displays the features of a nucleation-controlled process, the rate decreasing with increasing temperature (Figures 7–9).

The scatter in the data presented in Figure 7 is due not to poor accuracy in the measurements but rather to heterogeneity within the samples. The coefficient of determination (r^2) for the growth rate data (main direction) was 0.835 (20 data points). Figure 8 presents growth rate data for a single sample, and the scatter is significantly reduced (r^2 for main direction growth rate data was 0.974 (7 data points)). Regression analysis shows that the growth rate data best follow the growth rate equation valid for secondary nucleation (eq 7). This is also the case for the

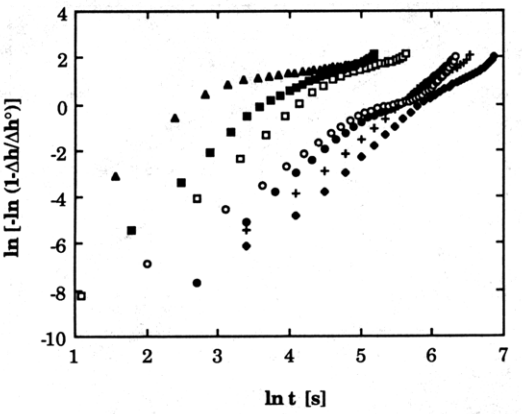

Figure 13. Avrami plots (according to eq 1) for HPX-C11 no. 1 obtained at different temperatures: 456.9 K (▲); 458.9 K (■); 460.9 K (□); 461.9 K (○); 462.9 K (●); 463.9 K (+); 464.9 K (◆).

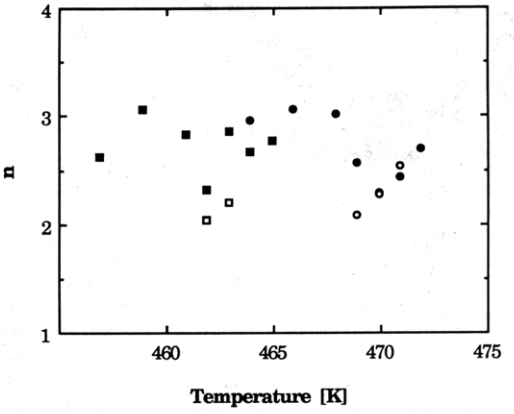

Figure 14. Avrami exponent value (n) plotted versus temperature for HPX-C11 no. 1 [rapid process (■); slow process (□)] and HPX-C9 (rapid process (●); slow process (○)].

$$G = G_0 \exp\{-K_g/[T(T^\circ_i - T)]\} \quad (7)$$

kinetic data obtained by DSC (Figure 9), although, as discussed later in this paper, other mechanisms give rise to a similar temperature dependence and are also possible. The factor K_g is a constant that depends on the mechanism and on the surface free energies (σ_i).

The growth rate data obtained by DSC is treated according to eq 8 see (Figure 9), which is a DSC equivalent of

$$(t_{0.4})^{-1} = C \exp\{-K_g/[T(T^\circ_i - T)]\} \quad (8)$$

of eq 7 ($t_{0.4}$ is the time for 40% conversion of the rapid process).

The K_g values presented in Table I demonstrate the similarity of the exothermal process recorded by DSC and the growth of the mesomorphic domains recorded by polarized-light microscopy. It is also evident that K_g is 20–30% lower for HPX-C9 than for HPX-C11. The growth along the chain axis occurs by a mechanism with a K_g value that is 2/3 of the value for the perpendicular growth.

The unique feature of the mosaic domains is the uniform chain orientation, which is essentially preserved during their growth. A relevant question that has to be addressed is whether the uniform chain orientation is also a characteristic on a suboptical microscopy level. Electron microscopy information concerning the detailed morphology is presently not available. If it is assumed that the uniform chain orientation is also present at molecular levels, it is very difficult to see how a well-defined secondary nucleation step may occur from a smooth

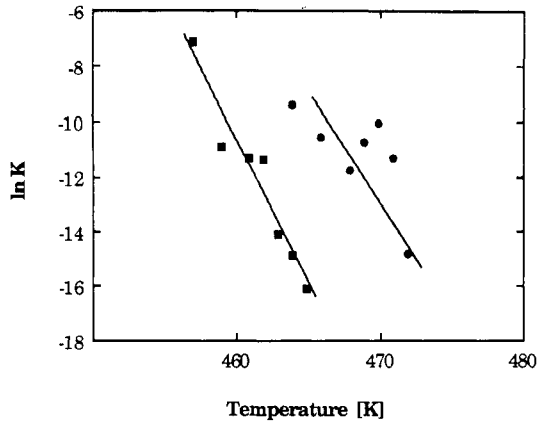

Figure 15. Logarithm of the Avrami constant K plotted versus temperature for the rapid process occurring in HPX-C11 no. 1 (■) and HPX-C9 (●).

mesophase surface (Figure 11). The free energy barrier associated with this process should be too extensive. Furthermore, a mesophase boundary which is smooth down to molecular levels is not a very realistic structure. The rigid-rod chains which are attached to the mesophase domain are of different length (molecular weight distribution), and a rough mesophase surface is a more probable alternative (Figure 11). Thus, the growth may occur without any net change in area of the phase boundary, i.e., under invariant surface roughness. Computer simulations performed on a polyethylene crystallization by a rough surface model show that the linear growth rate may follow the $1/\Delta T$ dependence found experimentally.[12]

The slower process displays a temperature dependence opposite to that of the rapid process, the rate increasing with increasing temperature (Figure 10). This process cannot thus be controlled by nucleation but is possibly a rearrangement of the smectic mesophase against a higher degree of perfection. Figure 10 indicates that the process follows the Arrhenius equation with an activation energy of about 400–850 kJ mol^{-1}. The data points used to determine the activation energy are few, and the difference recorded for the two different polymers may simply be due to scatter in the data.

Figures 12 and 13 show that both processes indeed follow the Avrami equation. The nucleation-controlled process is shifted along the ordinate in the Avrami plot with essentially the same slope, i.e., the same Avrami exponent, at the different temperatures. The data obtained for the Avrami constants n and K are presented in Figures 14 and 15.

The Avrami exponent for the rapid process is almost independent of temperature and varies for both polymers around an average value between 2.6 and 2.7. For the slower process the exponent is lower with a value near 2.0. The exponent in the Avrami equation was derived long ago for a number of different nucleation types and crystal growth types and geometries. An excellent review of this topic is given by Wunderlich.[13]

Some relevant features of nucleation and growth were obtained by polarized-light microscopy: (1) The growth rate is constant with time, which indicates that the growth is not controlled by diffusion. (2) There is a significant anisotropy in growth rate approaching almost 1 order of magnitude (Figures 7 and 8). Hence, the growth cannot be regarded as truly three-dimensional. (3) Nucleation is neither prefectly athermal nor perfectly thermal. The nucleation rate was found to decrease markedly with time, so that nucleation seems to be a "mixture" of athermal and thermal types and growth seems to be nucleation controlled (constant growth rate) and less than three-dimensional. This picture is consistent with the n values obtained. Wunderlich[13] reports $n = 2$ for athermal nucleation followed by two-dimensional growth and $n = 3$ for thermal nucleation followed by two-dimensional growth.

Conclusions

The transformation of the isotropic melt into the smectic mesophase is a nucleation-controlled process. The linear growth rate of the mesomorphic mosaic domains is constant with time and the logarithm of the growth rate follows a $1/[T(T^\circ_i - T)]$ dependence. The growth of the mesophase is highly anisotropic. The growth rate is greater in the chain axis direction than in the perpendicular direction. This observation is consonant with the average value between 2.6 and 2.7 for the Avrami exponent, which indicates a two-dimensional growth of the mesomorphic domains to follow a mixed athermal/thermal nucleation event.

A second process, which occurred at rates almost comparable with the formation of the smectic mesophase, displayed an Arrhenius temperature dependence with an activation energy of about 400–850 kJ mol^{-1}. This is indicative of a rearrangement of the smectic mesophase, which occurs without rate-controlling nucleation. Furthermore, the process followed the general Avrami equation with an exponent near 2.0.

High-temperature X-ray diffraction is presently being carried out, and the results, which further illuminate the mesomorphic structures and thus the exact nature of the two phase transitions, will be presented in a future paper.[14]

Acknowledgment. These studies have been financed by The National Swedish Board for Technical Development (STU) (Grant No. 86-03476P) and The Swedish Natural Science Research Council (NFR) (Grant K-KU No. 1910–300). The scholarship for H.J. from The Royal Institute of Technology, Stockholm, is gratefully acknowledged.

References and Notes

(1) Bhattacharya, S. K.; Misra, A.; Stein, R. S.; Lenz, R. W.; Hahn, P. E. *Polym. Bull.* **1986**, *16*, 465.
(2) Liu, X.; Hu, S.; Shi, L.; Xu, M.; Zhou, Q.; Duan, X. *Polymer* **1989**, *30*, 273.
(3) Hans, K.; Zugenmaier, P. *Macromol. Chem.* **1988**, *189*, 1189.
(4) Pracella, M.; De Petris, S.; Frosini, V.; Magagnini, P. L. *Mol. Cryst. Liq. Cryst.* **1984**, *113*, 225.
(5) Price, F. P.; Wendorff, J. H. *J. Phys. Chem.* **1971**, *75*, 2839.
(6) Price, F. P.; Frietzsche, A. K. *J. Phys. Chem.* **1973**, *77*, 369.
(7) Price, F. P.; Wendorff, J. H. *J. Phys. Chem.* **1972**, *76*, 276.
(8) Jonsson, H.; Werner, P.-E.; Gedde, U. W.; Hult, A. *Macromolecules* **1989**, *22*, 1683.
(9) Shaffer, T. D.; Jamaludin, M.; Percec, V. *J. Polym. Sci., Polym. Chem. Ed.* **1985**, *23*, 2913.
(10) Percec, V.; Nava, H.; Jonsson, H. *J. Polym. Sci., Polym. Chem. Ed.* **1987**, *25*, 1943.
(11) Hoffman, J. D.; Weeks, J. J. *J. Res. Natl. But. Stand.* **1963**, *A66*, 13.
(12) Sadler, D. M.; Gilmer, G. H. *Polymer* **1984**, *25*, 1446.
(13) Wunderlich, B. *Macromolecular Physics: Crystal Nucleation, Growth, Annealing*; Academic Press: New York, 1978; Vol. 2.
(14) Jonsson, H.; Gedde, U. W.; Hult, A.; Werner, P.-W., to be submitted for publication in *Macromolecules*.